1

Luminescence and a New Approach for Detecting Heat Treatment of Sapphire

Teerarat Pluthametwisute[1,2], Lutz Nasdala[2], Chutimun Chanmuang N.[2], Manfred Wildner[2], Eugen Libowitzky[2], Gerald Giester[2], E. Gamini Zoysa[3], Chanenkant Jakkawanvibul[4], Waratchanok Suwanmanee[4], Tasnara Sripoonjan[5], Thanyaporn Tengchaisri[6], Bhuwadol Wanthanachaisaeng[4] and Chakkaphan Sutthirat[1]

[1]Department of Geology, Faculty of Science, Chulalongkorn University, 10330 Bangkok, Thailand;

[2]Institut für Mineralogie und Kristallographie, Universität Wien, 1090 Wien, Austria;

[3]Mincraft Co**.**, 10370 Mount Lavinia, Sri Lanka;

[4]The Gem and Jewelry Institute of Thailand **(**Public Organization**)**, 10500 Bangkok, Thailand;

[5]G-ID Laboratories, Bangkok, 10120, Thailand;

[6]Science and Technology Park **(**STeP**)**, Chiang Mai University, 50200 Chiang Mai, Thailand**.**

Correspondence*:* Chakkaphan Sutthirat (email*:* chakkaphan.s@chula.ac.th)

Abstract. For decades, unravelling heat treatment of sapphire has been a challenging issue. The present study offers new aspects that support the detection of heat treatment of sapphire. Natural unheated sapphire is distinguishable from heated sapphire by its orange to red luminescence under long-wave ultraviolet (LWUV, 365 nm) light, whereas blue luminescence under short-wave ultraviolet (SWUV, 254 nm) light indicates their heated counterparts. UV-excited photoluminescence shows a linkage between a broad emission spectrum within the orange to red region and orange to red luminescence of natural unheated sapphire under LWUV illumination, as well as an emission spectrum around the green region and blue luminescence of heated sapphire under SWUV illumination. Furthermore, the presence of melt inclusions within dissolved silks may be used as an indicator of heat treatment of sapphire. It seems that Fourier-transform infrared (FTIR) spectroscopy alone is inadequate for distinguishing unheated and heated sapphire. The application of orange to red, and blue luminescence together with melt inclusions offer a novel and practicable procedure for more precise differentiation of unheated versus heated sapphire.

Keywords: gem; sapphire; heat treatment; luminescence

1 Introduction

Since the 1970s, Sri Lanka has maintained an outstanding record for its rich supply of gemstones (Soysa and Fernando, 1992). Among diverse corundum varieties, the so-called geuda sapphire is noteworthy, as it has been often subjected to high-temperature heat treatment to increase its value by enhancement of color and clarity (Ediriweera and Perera, 1989; Perera et al., 1991). Geuda sapphire is characterized by milky

39   and/or silky appearance. Heat treatment of corundum (ruby and sapphire) has the capacity to modify the

40   appearance of milkiness and asterism, color, and even the internal features (including mineral inclusions)

41   of the gemstones (Nassau, 1981; Ediriweera and Perera, 1989; Hughes, 1997, 2017; Kyi et al., 1999;

42   Pisutha-Arnond, 2017; Themelis, 2018). Temperature and duration of the heating process, as well as

43   reducing or oxidizing conditions, are the most significant factors influencing corundum's alterations

44   (Nassau, 1981; Emmett and Douthit, 1993; Peiris, 1993; Emmett et al., 2003; Hughes, 2017; Pisutha-

45   Arnond, 2017; Soonthorntantikul et al., 2019). Heat treatment can be classified as high- or low-temperature

46   according to the decomposition of rutile silks in corundum (Nassau, 1981; Emmett and Douthit, 1993;

47   Emmett et al., 2003; Hughes, 2017; Hughes and Perkins, 2019). The term low-temperature heat treatment

48   has been used (typically referred to as below 1000 °C) when rutile particles still reveal their original

49   structures. On the other hand, temperatures beyond 1350 °C denote high-temperature heat treatment when

50   rutile silks start to decompose and dissolve within the corundum host (Hughes, 2017; Themelis, 2018).

51   Consequently, internal diffusion (indicated by a colored halo surrounding the crystal inclusion), molten or

52   altered inclusions, and/or broken silk are strong indicators of high-temperature heat treatment. However,

53   low-temperature heat treatment can also produce various altered mineral inclusions (Kammerling et al.,

54   1990; McClure and Smith, 2000; McClure et al., 2010; Pisutha-Arnond, 2017; Soonthorntantikul et al.,

55   2019).

56   One of the first-rank challenges encountered by gemologists nowadays is the precise and

57   reliable identification of heat-treated ruby and sapphire. Blue luminescence under SWUV light has been

58   observed in heated sapphire some 50 years ago (Crowningshield 1966, 1970). This luminescence may also

59   extend into the green region (Nassau, 1981). It has been studied afterwards by numerous researchers (Evans,

60   1994; Wong et al., 1995a; Wong et al., 1995b; Hughes 1997; McClure and Smith, 2000; Page et al., 2010;

61   Alombert-Goget et al., 2016a; Alombert-Goget et al., 2016b; Hughes, 2017; Vigier et al., 2021a, b, 2023).

62   This phenomenon may relate to rutile inclusions in sapphire (Hughes, 2017). It should be mentioned that

63   most natural blue sapphires contain some exsolved rutile (TiO_2) in the form of silk and/or needle inclusions

64   (Sutthirat et al., 2006; Hughes, 2017). When these sapphire samples are heated, rutile dissolves gradually

65   at temperatures of about 1600 °C (Sutthirat et al., 2006), resulting in the incorporation of Ti^{4+} ions into the host

66   sapphire structure. After Ti^{4+} being exposed to SWUV light, they yield luminescence. However, blue

67   luminescence was not observed in both unheated and heated basaltic sapphire, possibly due to the abundant

68   presence of Fe^{2+} of basaltic origin that may strongly quench such blue luminescence (Soonthorntantikul et

69   al., 2019). More details will be discussed in this report. Furthermore, even though microscopic inclusions

70   have been the distinguishing characteristics of heated sapphire, identifying heat-treated sapphire remains

71   challenging (Crowningshield, 1966; Hughes, 2017). Spectroscopic techniques such as Fourier-transform

72   infrared (FTIR) spectroscopy have also been applied to detect heated sapphire. In some cases, the presence

73   or absence of specific FTIR features in the O-H absorption region (3100–3600 cm^{-1}) may serve as an

74   indicator of heat treatment (Smith, 1995; Beran and Rossman, 2006; Saeseaw et al., 2018); however, it is

75   probably not a conclusive evidence (Ediriweera and Perera, 1989; Perera, 1993; Sutthirat et al., 2006;

76   Cartier, 2009; Jaliya et al., 2020). The most efficient technique and key evidence enabling to identify heat-

77   treated sapphire is its blue luminescence (Crowningshield, 1966; McClure and Smith, 2000; Hughes, 2017;

78   Hughes and Perkins, 2019). However, sequential research on original brown silk inclusions and orange

79   luminescence in natural unheated sapphire in relation with blue luminescence in the heated counterparts

80   has never been reported accordingly. Therefore, this study should be the first research that represents an

81   innovative approach to observe both original silk inclusions and luminescence in sapphire and their change

82   after heating experiments.

83

84   **2   Materials and Methods**

85

86   Natural unheated geuda sapphire samples were separated into 3 groups: 1) high-density-

87   silk group; 2) low-density-silk group; and 3) silk-free group (Fig. 1). Using an Enraf-Nonius Kappa single-

88   crystal X-ray diffractometer (sXRD) with a CCD area detector, these samples were oriented (based on 10

89   frames at a crystal detector distance of 35 mm), cut and polished into wafers with surfaces parallel to the

90   c-axis. For electron probe micro-analysis (EPMA) slabs were coated with carbon for conductivity.

91   Heating experiments were conducted using a high-temperature electric furnace, Linn-

92   HT-1800-Vac. Heating was performed under ambient atmospheric conditions without any additional

93   oxygen buffer. Experimental conditions involved the maximum temperature of 1650 °C, which was

94   maintained for 10 hours, prior to natural cooling down in the furnace. A heating rate of 300 °C per hour

95   was set to reach the maximum temperature. To minimize surface contamination, the samples were placed

96   into a highly purified alumina (Al_2O_3) crucible.

97   Basic gemological data, such as refractive index, was measured by a gemological

98   refractometer with 1.81 refractive index liquid. Specific gravity was determined by a hydrostatic weighing

99   balance.

100   Micro-inclusions in all samples were investigated using an Olympus BX-series

101 microscope equipped with Olympus DP27 digital camera. The camera was operated using the Olympus

102 Stream micro-imaging software. Raman spectra of inclusions were acquired using a confocal micro-Raman

103 spectrometer Horiba Jobin Yvon LabRAM-HR Evolution. Using 473 nm laser excitation (15 mW at the

104 sample) and a 50×/0.50 objective lens, a spectral range of 100–1350 cm^{-1} Raman shift was recorded.

105 Wavenumber calibration was done using the Rayleigh line, resulting in wavenumber accuracy of better

106 than 0.5 cm^{-1}. A spectral resolution of ca. 1.2 cm^{-1} resulted from 800 mm focal length and an 1800

107 grooves/mm optical grating in the monochromator system. For more details see Zeug et al. (2018).

108   Chemical compositions of the samples were determined using a JEOL JXA 8100 EPMA.

109 Analytical conditions were set to 15 kV accelerating voltage and a probe current of about 2.5×10^{-8} A with

110 electron beam focussed to <1 μm. Natural mineral and synthetic oxide references were selected suitably

111 for calibration, including fayalite (Fe_2SiO_4) for Fe, wollastonite ($CaSiO_3$) for Ca, synthetic corundum

112 (Al_2O_3) for Al, synthetic periclase (MgO) for Mg, synthetic quartz (SiO_2) for Si, potassium titanyl

113 phosphate ($KTiOPO_4$) for K and Ti, synthetic manganosite (MnO) for Mn, synthetic eskolaite (Cr_2O_3) for

114 Cr, synthetic gadolinium gallium garnet ($Gd_3Ga_5O_{12}$) for Ga, and synthetic lead vanadium germanium

115 oxide for V. Counting times were 600 s peak and 300 s background for all elements. The K–α line was

116 analysed for all elements except for Ga where the L–α line was measured. Analytical crystals were selected

117 appropriately including thallium acid phthalate (TAP) crystal for Si and Al; pentaerythriol (PET) crystal

118 for Ti, Mg, K, and Ca; lithium fluoride (LIF) crystal for V, Cr, Ga, Fe, and Mn. The detection limit

4

119   (estimated from threefold background noise) is approximated at 0.005 % or 50 ppm. Three analytical spots

120   in each sample were selected for further analysis.

121   Polarized optical absorption (UV-VIS-NIR) spectra of samples were recorded on double-

122   sided polished crystal slabs in the spectral range of 35000-3500 cm^{-1}, covering the near ultraviolet (UV),

123   the visible (VIS) and the near infrared (NIR) ranges. The measurements were performed in the sample

124   chamber of a Bruker Vertex 80 FTIR spectrometer at 2 mm measuring spot, using a calcite Glan-prism

125   polarizer and appropriate combinations of light sources (Xe or W lamp), beam splitters (CaF$_2$-Vis/UV or

126   CaF$_2$-NIR), and detectors (GaP, Si or InGaAs diodes) to cover the desired spectral range. Hence, each full

127   spectrum was combined from three partial spectra: 1) 35000-18000 cm^{-1} with 40 cm^{-1} spectral resolution

128   and averaged from 256 scans; 2) 18000-9500 cm^{-1} with 20 cm^{-1} resolution and 256 scans; 3) 9500-3500

129   cm^{-1} with 10 cm^{-1} resolution and 128 scans.

130   Fourier-transform infrared (FTIR) spectra were acquired by means of a Bruker Tensor

131   27 FTIR spectrometer attached to a Bruker Hyperion microscope in the spectral range from 4000 cm^{-1} to

132   1600 cm^{-1}. A glowbar light source, a KBr beamsplitter, and a deuterated L-alanine doped triglycene

133   sulphate (dLATGS; Tensor27) or Hg-Cd-telluride (MCT) detector (Hyperion) were employed. The

134   spectral resolution was 4 cm^{-1}, sample and reference spectra were averaged from 128 scans.

135   Luminescence phenomena were observed and photo-captured both before and after heat

136   treatment. The images were obtained under LWUV (365 nm) illumination using a commercial UV lamp,

137   and under SWUV (254 nm) illumination by means of a DiamondView^{TM} device. Photoluminescence (PL)

138   spectra in the visible and NIR ranges were acquired using a confocal Horiba Jobin Yvon LabRAM-HR 800

139   spectrometer. Spectra were excited using the 325 nm emission of a He-Cd laser (ca. 10 mW at the sample

140   surface). The system was calibrated using emission lines of a Kr lamp. The spectral resolution was in the

141   range 0.07 nm (violet) to 0.02 nm (NIR range).

142

143   **3 Results**

144

145   **3.1 Heating-induced property changes and alteration**

146   Natural unheated geuda sapphire samples were separated based on the appearance of silk inclusions into

147   three distinctive groups, i.e., high-density-silk, low-density-silk, and silk-free specimens. Representatives

148   of natural unheated and their heated counterparts of all groups are shown in Fig. 1. All the samples ranged

149   from a specific gravity of 3.83 to 4.08 g/cm^3, and refractive indices of 1.760 to 1.770 falling within the

150   field of corundum's properties. After heating, most samples turned blue, varying from pale blue to dark

151   blue. Alteration was clearly observed in the geuda samples with high-density-silk inclusions (G03 and G04,

152   Fig. 1), which naturally showed brown silk and brown color banding/zoning. Moreover, a few samples in

153   this group also showed a natural blue appearance (G02, Fig. 8). Regarding sapphire samples with low-

154   density-silk inclusions, these stones (e.g., G18 and G21, Fig. 1) typically presented a milky appearance

155   with yellowish or brownish tints, which were obviously diminished after heating. On the other hand, the

156   silk-free group usually showed a slightly yellowish appearance (Fig. 1, samples G11 and G12). After the

157   heating experiment, they had changed slightly to a very pale blue color.

158

5

Figure 1. Representatives of natural unheated geuda sapphire samples within three separate groups, i.e.,
high-density-silk (G03, G04), low-density-silk (G18, G21), and silk-free (G11, G12) groups, and their
appearances after heating. Sizes of stones range between 0.4 and 12 mm.

3.2 Mineral chemistry

Chemical compositions of samples in the three distinct groups are summarized in Tables 1 to 3. The Al_2O_3
contents range between 98.2 and 99.5 wt%. Other elements are found as trace contents only, particularly
Fe, Ti, and Ga. Fe and Ti are essential coloring elements in sapphire. The high-density-silk group contained
the highest Fe contents of 0.32-0.36 wt% FeO, together with 0.02-0.04 wt% TiO_2 and <0.7 wt% Ga_2O_3.
The low-density-silk group had a high Ti content of 0.02-0.51 wt% TiO_2 with ≤0.06 wt% FeO and ≤0.8
wt% Ga_2O_3. The silk-free group contained 0.06-0.26 wt% FeO, ≤0.04 wt% TiO_2 and <1 wt% Ga_2O_3.

6

171 **Table 1.** Representative chemical compositions (EPMA results) and calculated mineral formulae of high-
172 density-silk sapphire samples.

Samples	G01	G02	G03	G04
Major oxides (wt%):				
SiO_2	0.00	0.00	0.45	0.40
TiO_2	0.02	0.02	0.04	0.03
Al_2O_3	99.0	98.7	98.9	98.7
V_2O_3	0.01	0.00	0.00	0.03
Cr_2O_3	0.00	0.02	0.03	0.00
Ga_2O_3	0.62	0.66	0.00	0.39
FeO_{total}*	0.32	0.33	0.36	0.36
MnO	0.02	0.00	0.00	0.02
MgO	0.00	0.00	0.01	0.01
K_2O	0.00	0.00	0.00	0.00
CaO	0.01	0.01	0.02	0.01
Total	100.0	99.8	99.8	100.0
Mineral formulae (apfu)**:				
Si	0.000	0.000	0.008	0.007
Ti	0.000	0.000	0.001	0.000
Al	1.990	1.989	1.985	1.982
V	0.000	0.000	0.000	0.000
Cr	0.000	0.001	0.000	0.000
Ga	0.007	0.007	0.000	0.004
Fe	0.013	0.014	0.005	0.005
Mn	0.000	0.000	0.000	0.000
Mg	0.000	0.000	0.000	0.000
K	0.000	0.000	0.000	0.000
Ca	0.000	0.000	0.000	0.000
Sum	2.010	2.011	1.999	2.000

173 * FeO_{total} = total Fe oxide, assuming all Fe to be ferrous

174 ** Calculated based on 3 O atoms per formula unit

175

176 **Table 2.** Representative chemical compositions (EPMA results) and calculated mineral formulae of low-
177 density-silk sapphire samples.

Samples	G06	G16	G18	G20	G21
Major oxides (wt%):					
SiO_2	0.00	0.00	0.11	0.00	0.00
TiO_2	0.04	0.27	0.37	0.51	0.02
Al_2O_3	99.0	98.5	98.4	98.3	98.6
V_2O_3	0.02	0.03	0.01	0.02	0.01
Cr_2O_3	0.00	0.06	0.00	0.02	0.00
Ga_2O_3	0.10	0.37	0.58	0.81	0.59
FeO_{total}*	0.00	0.06	0.06	0.06	0.05
MnO	0.01	0.00	0.00	0.00	0.01
MgO	0.02	0.02	0.01	0.01	0.02
K_2O	0.00	0.00	0.00	0.00	0.00
CaO	0.00	0.00	0.01	0.01	0.00
Total	99.2	99.3	99.6	99.7	99.3
Mineral formulae (apfu)**:					
Si	0.000	0.000	0.002	0.000	0.000
Ti	0.001	0.003	0.005	0.007	0.000
Al	1.997	1.989	1.984	1.981	1.992
V	0.000	0.000	0.000	0.000	0.000
Cr	0.000	0.002	0.000	0.001	0.000
Ga	0.001	0.004	0.006	0.009	0.007
Fe	0.000	0.002	0.002	0.002	0.002
Mn	0.000	0.000	0.000	0.000	0.000
Mg	0.001	0.001	0.001	0.000	0.001
K	0.000	0.000	0.000	0.000	0.000
Ca	0.000	0.000	0.000	0.000	0.000
Sum	2.001	2.003	2.000	2.000	2.002

178 * FeO_{total} = total Fe oxide, assuming all Fe to be ferrous

179 ** Calculated based on 3 O atoms per formula unit

180

181 **Table 3.** Representative chemical compositions (EPMA results) and calculated mineral formulae of silk-

182 free sapphire samples.

Samples	G07	G11	G12	G14	G22	G23
Major oxides (wt%):						
SiO_2	0.01	0.13	0.06	0.00	0.00	0.00
TiO_2	0.03	0.04	0.03	0.00	0.04	0.01
Al_2O_3	98.7	98.7	98.8	99.5	98.2	98.7
V_2O_3	0.00	0.02	0.00	0.00	0.00	0.00
Cr_2O_3	0.00	0.00	0.01	0.00	0.00	0.00
Ga_2O_3	0.71	0.00	0.00	0.15	0.78	0.94
FeO_{total}*	0.06	0.26	0.08	0.10	0.22	0.13
MnO	0.01	0.02	0.00	0.01	0.02	0.00
MgO	0.00	0.02	0.00	0.00	0.00	0.00
K_2O	0.00	0.01	0.00	0.00	0.00	0.00
CaO	0.02	0.00	0.02	0.01	0.01	0.01
Total	99.6	99.2	99.0	99.8	99.3	99.8
Mineral formulae (apfu)**:						
Si	0.000	0.002	0.001	0.000	0.000	0.000
Ti	0.000	0.001	0.000	0.000	0.001	0.000
Al	1.991	1.993	1.997	1.997	1.988	1.988
V	0.000	0.000	0.000	0.000	0.000	0.000
Cr	0.000	0.000	0.001	0.000	0.000	0.000
Ga	0.008	0.000	0.000	0.002	0.009	0.010
Fe	0.002	0.011	0.003	0.004	0.009	0.005
Mn	0.000	0.000	0.000	0.000	0.000	0.000
Mg	0.000	0.001	0.000	0.000	0.000	0.000
K	0.000	0.000	0.000	0.000	0.000	0.000
Ca	0.000	0.000	0.000	0.000	0.000	0.000
Sum	2.002	2.009	2.003	2.003	2.007	2.004

183 * FeO_{total} = total Fe oxide, assuming all Fe to be ferrous

184 ** Calculated based on 3 O atoms per formula unit

185

3.3 Microscopic features

Negative crystals with/without CO_2 gas bubble appeared to be the common internal feature as well as mineral inclusions (e.g., oligoclase feldspar, calcite, and muscovite) that were usually found in these sapphire samples. Additionally, brown silk inclusions were clearly recognized in high-density-silk and low-density-silk groups. Fig. 2 presents the most common micro-inclusions found in these samples. Micro-Raman spectroscopy was applied for identification of CO_2 and mineral inclusions. However, brown silk inclusions, usually oriented along the color banding/zoning (Fig. 3a), were very tiny (less than 1 µm in diameter) and rather difficult to be identified by any technique. These silk inclusions were typically needle shaped, however, thin, irregular, or flaky platelets of silk inclusions (Fig. 3c) also appeared in these sapphire samples.
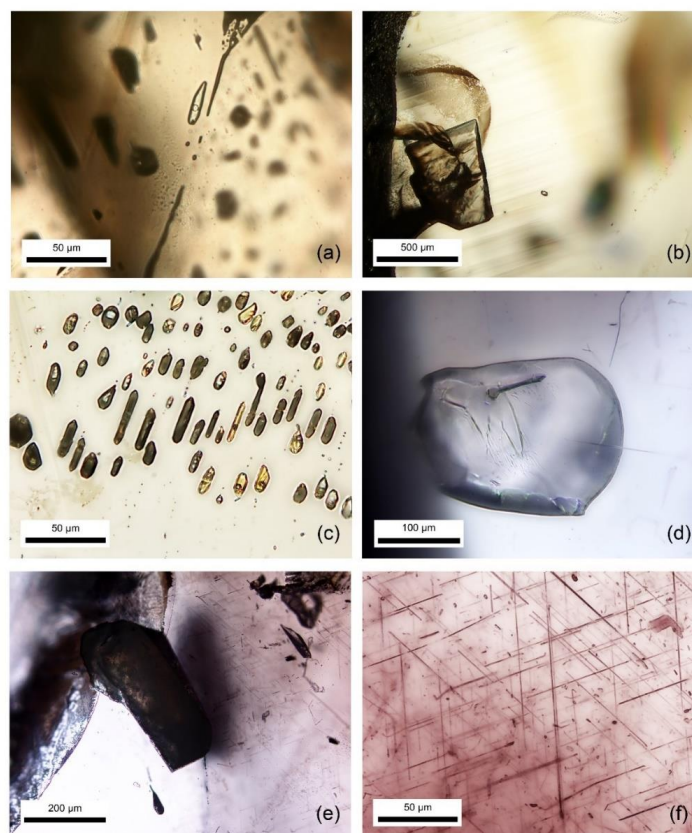
Figure 2. Photomicrographs of inclusions including CO_2-containing negative crystals **(a)**, calcite **(b)**, cluster of negative crystals **(c)**, oligoclase **(d)**, muscovite **(e)**, and brown silks **(f)** in natural unheated sapphire.

10

202   After high-temperature heating, molten surfaces (Fig. 3e) and decomposed crystal

203   inclusions were commonly observed in these sapphire samples. The most notable alteration was also

204   detected in the initial area of brown silks (Fig. 3a), which exhibited distinct bluish color banding/zoning

205   (Fig. 3b) after heating.

206
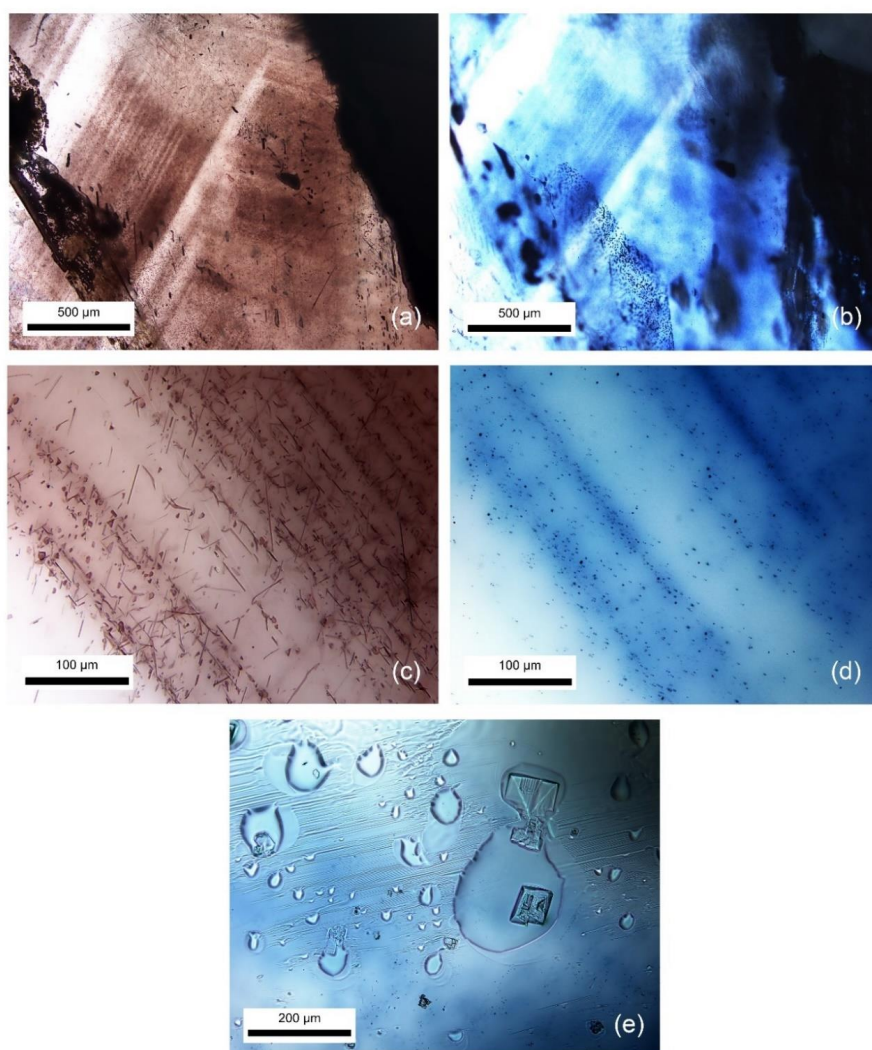
207

208   **Figure 3.** Brown banding **(a)** with irregular platy brownish flakes and tiny needles **(c)** in natural unheated

209   sapphire samples turned into blue color banding **(b)** with blue dots **(d)** after heating. Melted surface **(e)** was

210   also observed after heat treatment.

211

212   The brown silks (Fig. 3c) experienced a transformation upon heating into blue dots (Fig.
213   3d). Additionally, melt inclusions among blue dots were likely developed by melting of brown silks with
214   collaborative reaction of the sapphire host, which have never been reported elsewhere, becoming
215   significantly noticeable and useful for indicating heat treatment of sapphire (Fig. 4).
216
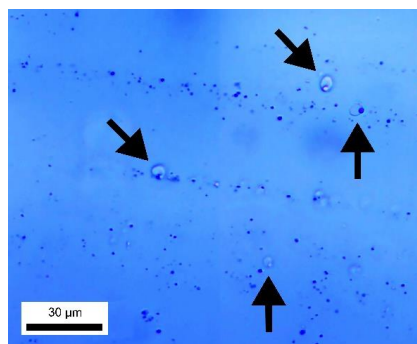
218   **Figure 4.** Melt inclusions (arrows) among blue dots transformed from silk inclusions in sapphire after
219   heating.
220

3.4   Optical (UV-VIS-NIR) spectroscopy

222   The optical spectra of representative sapphire samples are presented in Fig. 5. Absorption peaks at 374,
223   388, and 450 nm, as well as bands around 580 and 880 nm, were observed. Optical spectra have been
224   studied on unheated and heated sapphire by numerous previous researchers (e.g., Ediriweera and Perera,
225   1989; Perera et al., 1991; Emmett and Douthit, 1993; Hughes, 1997; Kyi et al., 1999; Emmett et al., 2003;
226   Sripoonjan et al., 2014; Hughes, 2017; Pisutha-Arnond, 2017; Themelis, 2018; Palke et al., 2019;
227   Soonthorntantikul et al., 2019; Dubinsky et al., 2020). The 374, 388, and 450 nm peaks as well as the 880
228   nm band were proposed to be attributed to Fe, the 580 nm band to the Fe-Ti pair. After heating, all samples
229   showed a significant increase in the main Fe-Ti pair related absorption band at around 580 nm (Figs. 5a-c),
230   whereas Fe-Fe related absorption at around 880 nm was obviously increased in some samples (i.e., Figs.
231   5a and 5c). The intensified absorption of the 580 nm band in these samples is referred to an increase of Fe-
232   Ti pairs after heating which leads to enhanced blue coloration in heated sapphires.
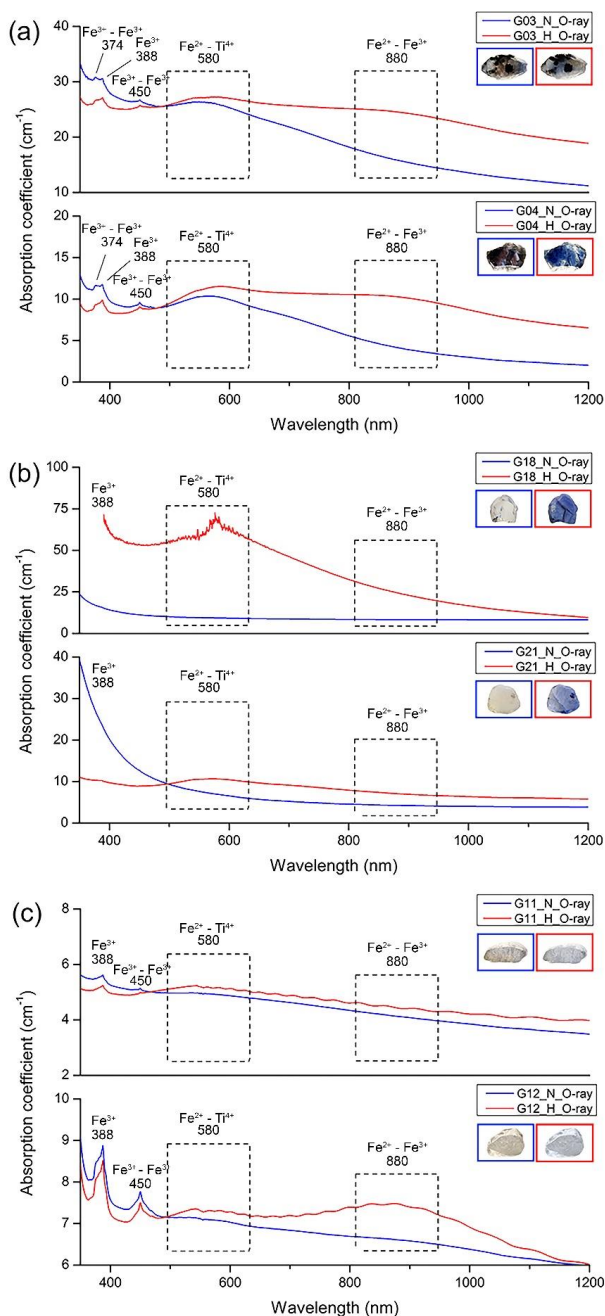
Figure 5. Optical absorption spectra of untreated (blue lines) and heated (red lines) samples: **(a)** high-density-silk group (G03, G04); **(b)** low-density-silk group (G18, G21); **(c)** silk-free group (G11, G12). Sizes of stones range between 0.4 and 12 mm.

238   Spectral characteristics of corundum containing Fe^{3+} ions exhibit a high degree of

239   complexity. It is noteworthy that Fe^{3+} has electron configuration d^5 resulting in a crystal field spectrum

240   with ground state $^6A_1$ (Ferguson and Fielding, 1972). Small peaks at 374 nm ($^4E^b$) and 450 nm ($^4A_1,^4E^a$)

241   should be attributed to the enhanced absorption of Fe^{3+}-Fe^{3+} pairs (McClure, 1962; Ferguson and Fielding,

242   1971; Krebs and Maisch, 1971; Ferguson and Fielding, 1972) as well as a weak broadband absorption at

243   540 nm ($^4T_2$) which could not be seen in this work. The distinct peak observed at a wavelength of 388 nm

244   ($^4T_2{}^b$) (Krebs and Maisch, 1971) is linked to the individual Fe^{3+} ions. This, however, does not rule out the

245   possibility of a higher-order cluster with extra ions or other point defects (Emmett et al., 2003).

246   Additionally, there is also a broad band at a wavelength of 330 nm ($^4T_1{}^b$) which is interpreted as a Fe^{3+}-

247   Fe^{3+} pair absorption (Ferguson and Fielding, 1972). This is also present in the spectra of heated samples

248   G03 and G04, as well as in all spectra of sample G12 in this study. In trace contents both Fe^{2+} (d^6) and Ti^{4+}

249   (d^0) ions alone do not exhibit any absorption in corundum in the visible range (Townsend, 1968); on the

250   other hand, Fe^{2+}-Ti^{4+} pairs ($t_2 \rightarrow {}^2E$) (Ferguson and Fielding, 1971) may yield a broad band absorption

251   around 580 nm (E⊥c), or 700 nm (E∥c) (Dubinsky et al., 2020). The Fe^{2+}-Fe^{3+} pair gives rise to the broad

252   absorption band at ca. 880 nm (Fig. 5; Ferguson and Fielding, 1972).

253

254   **3.5 FTIR spectroscopy**

255   Fourier-transform infrared (FTIR) spectra of most samples yielded identical patterns within the range of

256   1600-4000 cm^{-1} (Fig. 6). They usually showed CO_2 peaks (at 2339 and 2360 cm^{-1}), as well as C-H stretching

257   related peaks (at 2856 and 2925 cm^{-1}), likely from turbidity (Fig. 6, blue lines), in accordance with Hughes

258   (2017) and Soonthorntantikul et al. (2021). However, O-H stretching of boehmite/diaspore peaks (at 1975

259   and 2105 cm^{-1}) (Delattre et al., 2012; Sun et al., 2015; Choi et al., 2017; Filatova et al., 2021;

260   Soonthorntantikul et al., 2021) was only observed in sample G03 from the high-density-silk group (Fig. 7a,

261   blue line). Weak absorption features of O-H stretching from H_2O (broad band at ca. 3400 cm^{-1}) and OH

262   groups (ca. 3600 – 3700 cm^{-1}) were only found in the untreated samples (blue lines), see Fig. 6a.

263

264
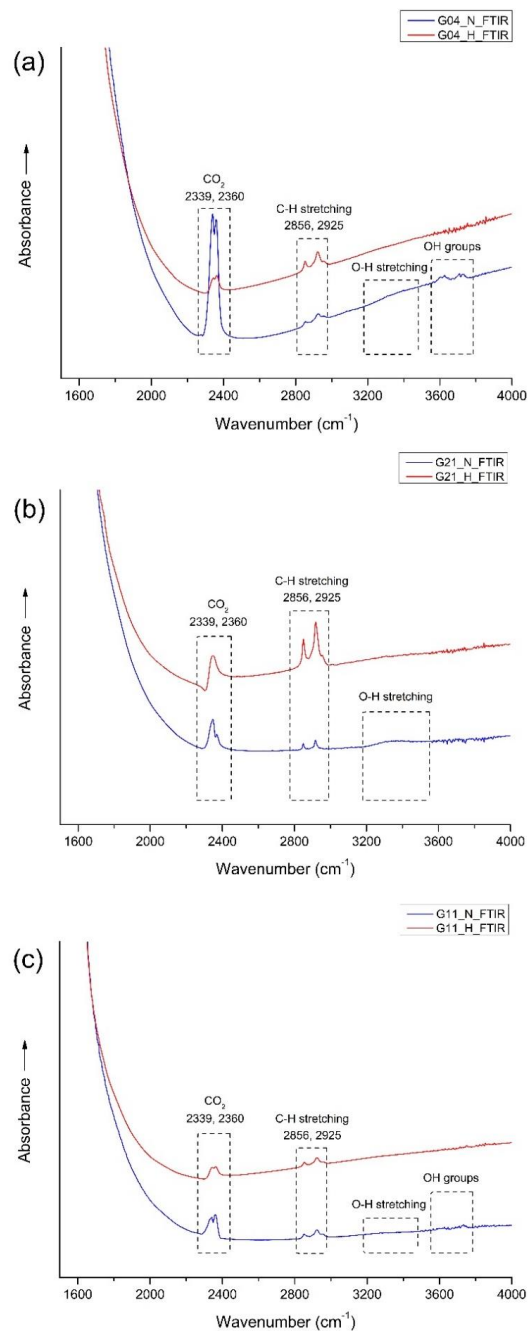
Figure 6. FTIR spectra before (blue lines) and after (red lines) heating experiments of representative

samples G04, G21, and G11 of the high-density-silk group **(a)**, low-density-silk group **(b)**, and silk-free

group **(c)**, respectively.

268

269   After heating, boehmite/diaspore-related absorption peaks (only observed in sample G03

270   of the high-density-silk group, Fig. 7a) at 1975 and 2105 cm^{-1} disappeared. In contrast, the 3309 cm^{-1}

271   hydroxyl (O-H) absorption, which was not present in any natural sample before heating, appeared only in

272   sample G18 of the low-density-silk group after heating (Fig. 7b, red line). It should also be mentioned that

273   the presence of CO_2 peaks at 2339 and 2360 cm^{-1}, as well as the C-H stretching related peaks at 2856 and

274   2925 cm^{-1} of all samples remained the same after heating. In contrast, their intensities vary dramatically

275   (see Figs. 6 and 7).

276
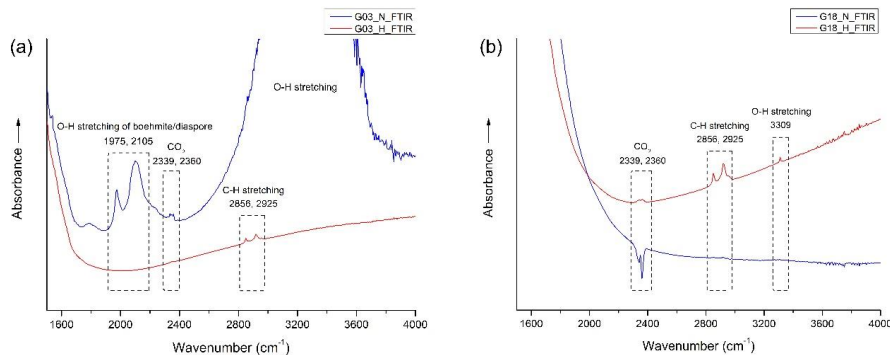
277

278   **Figure 7.** FTIR spectra before (blue lines) and after (red lines) heat treatment of samples G03 of high-

279   density-silk group **(a)** and G18 of low-density-silk group **(b)**.

280

281   To detect the heat treatment in corundum, FTIR spectroscopy is a recommended tool. In

282   some circumstances, the presence or absence of certain FTIR features in the O-H absorption region (3100-

283   3600 cm^{-1}) could be used as an indicator of heat treatment (Smith, 1995; Beran and Rossman, 2006;

284   Saeseaw et al., 2018; Saeseaw et al., 2020). For example, the presence of the 3309 cm^{-1} FTIR absorption

285   peak was used as an indicator of heated corundum (Hughes and Perkins, 2019; Saeseaw et al., 2020;

286   Soonthorntantikul et al., 2021). However, there were some inconsistencies presented recently: in some

287   cases the 3309 cm^{-1} peak was also found in unheated sapphire, thus it is not a reliable indicator of heat

288   treatment (Hughes, 1997, 2017; Hughes and Perkins, 2019; Saeseaw et al., 2020; Soonthorntantikul et al.,

289   2021).

290   In this study, an absence of O-H absorption in the 3100-3600 cm^{-1} range in all natural

291   geuda sapphire samples, together with the development of a weak absorption at 3309 cm^{-1} upon heating in

292   only one of the samples (see Fig. 7b, red line), address the limitation to differentiate unheated and heated

293   sapphire by FTIR spectroscopy. Furthermore, heat treatment employed in this study did not involve the use

294   of any additional gases, such as hydrogen, to create a reducing atmosphere within the furnace. Despite this,

295   the 3309 cm^{-1} absorption band was seen after the heating process. This might be in accordance with an

296   explanation proposed earlier by Notari et al. (2018).

297   The controversy of the presence of an O‑H peak in the FTIR spectrum in unheated and

298 heated sapphire could be attributed to an inherent hydrogen content of the corundum. Hydrogen was found

299 in corundum, primarily in the form of alumina hydrates (Notari et al., 2018). These hydrates could release

300 hydrogen through de‑hydroxylation at temperatures as low as approximately 450 °C. Additionally,

301 hydrogen was present in the air as H_2O, which can be split at temperatures around 900 °C to produce

302 hydrogen gas (H_2) and oxygen gas (O_2) through the reaction $2H_2O \rightarrow 2H_2 + O_2$ (Notari et al., 2018).

303

304 **3.6 Photoluminescence spectroscopy**

305   Photos presenting luminescence of some samples both before and after heat treatment are

306 shown in Fig. 8. Before heating, all natural sapphire samples were inert to SWUV light; moreover, all low-

307 density-silk and silk-free samples exhibited orange to red luminescence under LWUV light (Fig. 8). After

308 heating, all low-density-silk and silk-free samples, exhibited intense blue luminescence under SWUV

309 whereas their initial orange to red luminescence under LWUV excitation turned into a strong purplish red

310 luminescence (Fig. 8, samples G06 and G20 in particular). In summary, the high-density-silk samples were

311 all inert to SWUV and LWUV excitation both before and after heating. Notably under LWUV light, an

312 initial orange to red luminescence of a few samples from the silk-free group was drastically reduced after

313 heating (e.g., G23 in Fig.8).

314

315
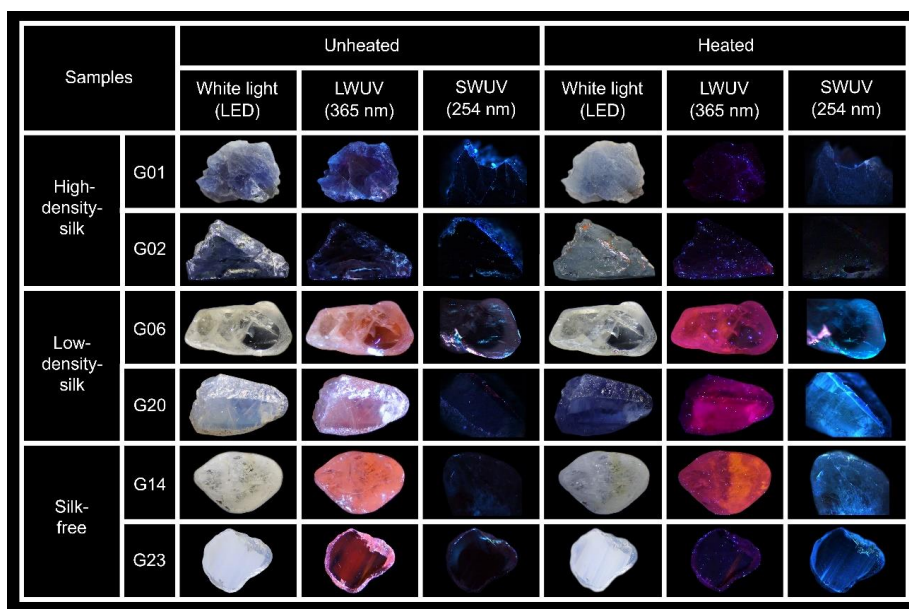
Figure 8. Representatives of high‑density‑silk (G01, G02), low‑density‑silk (G06, G20), and silk‑free
(G14, G23) groups under LWUV and SWUV illumination before and after heating. Sizes of stones range
between 0.4 mm and 12 mm.

319

320   The UV-excited photoluminescence (PL) spectra showed that all the unheated and heated

321 sapphire samples have an identical feature of two narrow peaks of trace Cr^{3+} lines at around 692.8 and

322   694.2 nm (Fig. 9) that are assigned to the spin-forbidden $^2E \rightarrow {}^4A_2$ relaxation of trace Cr^{3+} (Nelson and

323   Sturge, 1965). However, the Cr^{3+} lines of some samples (Fig. 9c) are too weak to be visible within the noise

324   of a broad and strong emission band. All unheated sapphire samples showed a similar emission band in the

325   orange to red region centered around 630-650 nm (Fig. 9a-c, blue line). Remarkably, this appears to be

326   associated with orange to red luminescence under LWUV light, as noted by (Segura, 2013; Vigier et al.,

327   2021a, b, c; Vigier and Fritsch, 2022). Despite having the emission band around 630-650 nm, only unheated

328   sapphires with high-density-silk appeared inert under LWUV illumination while the others revealed orange

329   to red luminescence.

330   After heating, significant alteration in the emission band was observed, as depicted by

331   the red lines in Fig. 9a-c. The photoluminescence spectra of sample G03 from the high-density-silk group

332   exhibited a notable reduction in the emission band through the visible region (Fig. 9a, red line). This went

333   along with a lack of luminescence both under SWUV and LWUV excitation, whereas sample G12 (silk-

334   free group) demonstrated a slight increase of the emission band in the orange to red region (Fig. 9c, red

335   line). More details are given in the discussion part below.

336   In contrast to the other groups, after heating, sample G21 of the low-density-silk group

337   (Fig. 9b, red line) exhibited a significant emission band in the green region at around 525 nm. Note that

338   this broad emission is excited with the 325 nm laser (Fig. 9) but does not seem to affect significantly the

339   emission colors observed under SWUV (254 nm) and LWUV (365 nm) excitation (Fig. 8). For a

340   discussion of the possibly strong dependence of emission intensity (and color) on the excitation

341   wavelength see for instance Zeug et al. (2022). Likewise heated sapphire has been proposed to have an

342   emission band in the blue region, which corresponds to blue luminescence under SWUV light (Nassau,

343   1981; Hughes, 2017; Vigier et al., 2023).

344

345
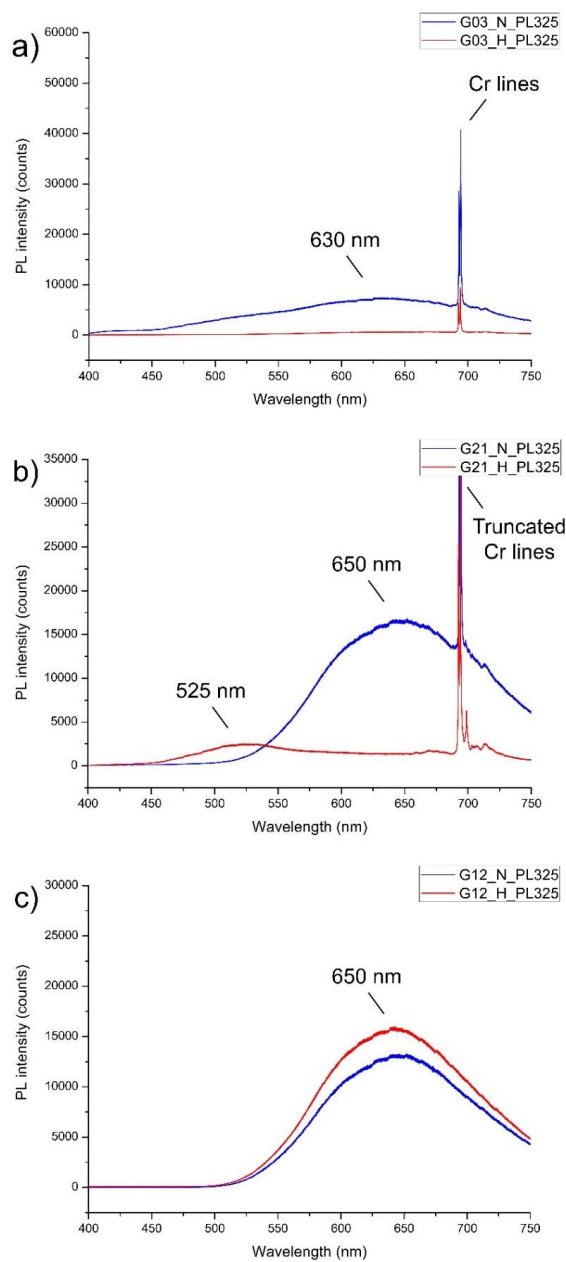
Figure 9. Representative photoluminescence (UV-excited) spectra before (blue lines) and after (red lines)
heating of sample G03 of high-density-silk group **(a)**, sample G21 of low-density-silk group **(b)**, and
sample G12 of silk-free group **(c)**.

349

19

4 Discussion

4.1 Silk inclusions and coloration of sapphire

Studies addressing brown silk inclusions in corundum are scarce. Soonthorntantikul et al. (2021) reported a mix of whitish silk and irregular/flaky/platelet-like brownish silk inclusions in corundum from Mogok. Brown silk was ascribed as presumable ilmenite ($FeTiO_3$) which is noticeable in high-Fe sapphire, whereas white silk was suggested to consist of rutile (TiO_2). The brown silks seen in our sapphire samples are likely ilmenite, which is supported by their irregular/flaky/platelet-like brownish appearance and their high Fe and Ti contents (note that the highest quantity of Fe was found in the high-density-silk group). Ilmenite decomposition upon heat treatment does result in Fe and Ti migration into the host sapphire and subsequently causes blue coloration. In particular, the decomposition of brown silks during heat treatment induces the formation of blue dots, which is a result of the Fe^{2+}-Ti^{4+} pairing formation. Upon closer inspection using a high-resolution microscope, these blue dots reveal distinct micro-inclusions as melt inclusions (with size of ≤1 µm, see Fig. 4), which have never been documented before. However, it should be noted that these melt inclusions are possibly derived from the decomposition of silks.

This work focuses only on blue coloration in sapphire which mainly relates to the Fe^{2+}-Ti^{4+} pair, as initially noted by Townsend (1968), followed by Mattson and Rossman (1988), Moon and Phillips (1994), and Emmett et al. (2003). Ti exhibits electron-donor properties, whereas Fe may function as an electron acceptor. When occupying neighboring Al^{3+} positions, absorption due to intervalence charge transfer between such donor-acceptor pairs may occur (details reported by Emmett et al., 2003 and Monarumit et al., 2023).

It should also be mentioned that Ti^{4+} ions do not exhibit any absorption characteristics in the visible spectrum when considered individually. The Ti^{4+} ion has a closed-shell electron configuration, whereas the Fe^{2+} ion mainly absorbs wavelengths within the near infrared and low-energy visible regions. In contrast, when Fe^{2+} and Ti^{4+} ions are situated on neighboring structural sites, notable absorption bands develop across the visible and near-infrared spectral regions. These Fe^{2+}-Ti^{4+} pairs exhibit a band center at around 580 nm (see Fig. 5) when the electric field vector E is perpendicular to the crystallographic c-axis (E⊥c), but a peak at 700 nm is seen when the electric field vector E is parallel to the crystallographic c-axis (E∥c) (Dubinsky et al., 2020). Although the theory of the energy levels of an individual transition metal ion inside a crystal has been extensively explored, the corresponding theory for ion pairs or clusters within a crystal remains underdeveloped (Dubinsky et al., 2020).

In this study, the natural unheated geuda sapphire samples were placed in atmospheric conditions and subjected to a maximum temperature of 1650 °C for a duration of 10 h. According to the samples presented in Fig. 1, samples G03 and G04 with high-density-silk inclusions exhibited a noticeable increase in blue coloration, particularly around the area of brown silks and brown color banding/zoning, after heating. On the other hand, the initial blue patch (e.g. samples G01 and G02) became paler blue after heating, which might be due to the breakage of initial Fe-Ti pairs in those areas. The other groups, which have yellowish and/or milky appearances, revealed an increase in blue color after heating (samples G12 and G18, Fig. 1). This blue coloration is attributed to two distinct factors, notably the dissolving of silk inclusions and a subsequent charge transfer mechanism (Emmett and Douthit, 1993; Hughes, 1997, 2017;

20

390   Nassau, 1980, 1981; Themelis, 2018). The process of charge transfer (Ferguson and Fielding, 1972; Nassau,

391   1981) is described as:

392    $Fe^{2+} + Ti^{4+} \rightleftarrows Fe^{3+} + Ti^{3+}$ (1)

393   It is important to note that the blue color observed in sapphire could also be produced

394   with the application of heat in oxidizing conditions. In recent studies, the possibility of employing Fe^{2+}-

395   Fe^{3+} charge transfer as an alternate method for blue coloration has also been mentioned (Nikolskaya et al.,

396   1978; Schmetzer and Kiefert, 1990; Häger, 1992, 2001; Sripoonjan et al., 2014; Pisutha-Arnond, 2017).

397   However, it is necessary to emphasize that this approach was considered highly improbable (Nassau, 1981).

398   Nevertheless, previous studies have indicated that a minor proportion of geuda sapphire from Sri Lanka

399   and geuda-like sapphire from Mogok in Burma revealed an alteration in color to blue when subjected to

400   heating in an oxidizing environment (Hughes, 1997, 2017; Kyi et al., 1999), which is in complete

401   contradiction to the treatment method employed for the geuda sapphire in a reducing condition. The

402   appearance of certain stones displaying a blue coloration under oxidizing conditions might be attributed to

403   the presence of ilmenite silks, which is composed of Fe and Ti, with Fe in its reduced Fe^{2+} state (Hughes,

404   1997). Therefore, it is unnecessary to reduce Fe^{3+} to Fe^{2+} ions to generate the Fe^{2+}-Ti^{4+} pairs that are

405   responsible for the manifestation of the blue color. Hence, the blue areas have a substantial concentration

406   of Fe ions in form of Fe-Ti pairs, derived from the decomposed ilmenite silk inclusions.

407   According to Nassau (1981) and Koivula (1987), the presence of blue dots in heated

408   sapphire is attributed to remains of dissolved silk inclusions and internal cation diffusion. The diffusion

409   process is positively correlated with temperature and duration of heat treatment (Nassau, 1981). Despite

410   the slow diffusion rates of Fe and Ti, the distances across are extremely short, i.e., just a few micrometers

411   (Nassau, 1981). Consequently, a potential Fe-Ti combination within the corundum's lattice may generate

412   the blue dots.

413   The presence of melt inclusions among the blue dots after high-temperature heating

414   might be due to the decomposition of brown silk and its solubility into the host sapphire as demonstrated

415   by Jung et al. (2009). They predicted a phase relationship within the Al_2O_3-Ti_2O_3-TiO_2 system based on

416   experimental data and thermodynamic calculation. Consequently, they suggested that a liquid phase (the

417   composition of the liquid inclusion phase varies significantly between Al_2O_3 and Ti_3O_5) could possibly be

418   present at a temperature of 1600 °C and slightly below, which is close to the heating temperature (1650 °C)

419   of our experiment. Silk inclusions as represented by Ti_2O_3-TiO_2 components may have dissolved into the

420   host sapphire (Al_2O_3 component), and produced a proper composition of solution which could be melted

421   partially at ≤ 1650 °C. Some of these melts can be preserved as inclusions after cooling down.

422

423   **4.2   Luminescence of sapphire**

424   Luminescence of corundum may be assigned to two types, namely (a) emissions of

425   impurity-related centers such as Ti^{4+} (commonly known) and (b) emissions of defect-related centers, which

426   typically involve either vacancies, such as oxygen (O) or aluminum (Al) vacancies known as F center

427   (color center; from the German "*Farbzentrum*"), or interstitials (Al_i and O_i), possibly trapped at impurities

428   (less known), or both (Viger et al., 2021a-c). This means that defect-related emission centers in corundum

429   refer to an inconsistency in the atomic arrangement limited to one or a few atoms (often called color-

21

430   centers). O vacancies (or electron holes) are sometimes called hole centers, because the holes simply

431   designate the absence of an electron. The holes are sometimes filled with one or two electrons in order to

432   maintain electroneutrality (Vigier et al., 2021a).

433   As presented in Fig. 8, a notable orange to red luminescence is easily noticeable under

434   LWUV excitation in most unheated sapphire samples, except for those of the high-density-silk group,

435   which appear inert. After heat treatment, the orange to red luminescence that is initially observed in all

436   samples of the low-density-silk group and many samples of the silk-free group turns into a purplish-red

437   luminescence. In contrast, no orange to red or purplish red luminescence is observed in any sample of the

438   high-density-silk group both before and after heating.

439   The origin of orange to red luminescence in sapphire remained controversial, with

440   varying ideas among researchers (Vigier et al., 2021a, b, 2023). The occurrence of orange luminescence

441   has been documented in some previous studies (e.g. Spencer, 1927; Kane, 1982; Emmett et al., 2003;

442   Fritsch et al., 2003). In the beginning, it was hypothesized that this luminescence is associated with the

443   geographic origin of yellow sapphire from Sri Lanka (Webster, 1984). Subsequently, Segura (2013)

444   presented an alternative argument to this notion, suggesting the presence of orange luminescence in various

445   colors of corundum, regardless of treatment or synthetic origin, might be attributed to the existence of some

446   defects. However, the orange to red luminescence observed in our study (characterized by a broad emission

447   band) seems to be associated with complex defect-related centers. As previously stated, orange to red

448   luminescence was proposed to be attributed with an F center or defect characterized by the occurrence of

449   two O vacancies (Vigier et al., 2021a, b). An O vacancy refers to the absence of an O atom in the structure.

450   It has the potential to remain an empty vacancy or to incorporate one or two unpaired electrons (Vigier et

451   al., 2021a, b).

452   However, it is possible that these defects may originate from boehmite/diaspore, which

453   undergo oxidation (Strange et al., 2022), dehydration (Gog, 2021), or dehydroxylation (Ananthakumar et

454   al., 1998) at temperatures exceeding 400 °C (Vlaskin et al., 2016). This process occurs through the

455   decomposition of $2AlO(OH) \rightarrow Al_2O_3 + H_2O$ (Kloprogge et al., 2002; Sifontes et al., 2019). Therefore,

456   when subjected to heating, these hydrated aluminas decompose and expell water (Samadhi et al., 2011).

457   This could result in the development of defects related to dehydration (Gog, 2021), which may be linked to

458   the F center as mentioned above.

459   Furthermore, it is important to note that the orange to red luminescence is not attributed

460   to any impurities (Vigier et al., 2021a, b). In addition, the absence of noticeable luminescence in high-

461   density-silk sapphire samples (see Fig. 8), both before and after heat treatment, can be attributed to the

462   presence of significant amounts of brown silks (ilmenite, $FeTiO_3$), where Fe^{2+} is suggested to play an

463   important role to suppress luminescence. This contrasts with samples of the low-density-silk and silk-free

464   groups, which exhibit more distinct orange to red luminescence both before and after heating. Even though

465   an orange to red luminescence of a few samples (e.g., G23) decreases after heating, increasing of orange to

466   red luminescence to a purplish red luminescence in most samples upon heating is generally observed (Fig.

467   8). This might be due to the remaining of altered, complex defect-related centers in the sapphire lattice as

468   mentioned earlier whereas the disappearance of orange to red luminescence in a few samples (see Fig. 8,

469   sample G23) might be due to the disappearance of defects after heating. Moreover, the orange luminescence

470   was proposed to be seen generally in colorless areas (Segura, 2013), which were described later on as low

471   Fe-containing areas (Notari et al., 2003). Therefore, Fe^{2+} serves as a quencher of luminescence for

472   emissions in the orange and red spectral range (Andrade et al., 2008; Norrbo et al., 2016; Vigier et al.,

473   2021a, b, c, 2023; Vigier and Fritsch, 2022). However, an exact clarification has never been established.

474   Regarding blue luminescence, it has been observed that upon exposure to SWUV light,

475   all natural unheated sapphire samples appeared inert. After heating, apart from high-density-silk sapphire,

476   a distinct blue luminescence has been detected throughout most heated sapphire samples (Fig. 8). It was

477   previously suggested that luminescence in sapphire is not noticed until they are heated up to a temperature

478   of 1000 °C (Hughes and Perkins, 2019). At this point, the discernible blue luminescence observed in

479   sapphire has been linked to the detection of heat treatment. This blue luminescence was proposed to be

480   attributed to the presence of silk (Hughes and Perkins, 2019) since the majority of natural blue sapphire

481   usually show the exsolved silk, which is composed of TiO_2. Notably, despite the relatively low Ti

482   concentration (0.02-0.03 wt% oxide) in comparison to Fe (0.05-0.08 wt% oxide) in some samples (e.g.,

483   G12 and G21 of the silk-free and low-density-silk groups, respectively), this blue luminescence is still

484   detected. Moreover, the absence of blue luminescence in high-density-silk samples (Fig. 8, sample G02) is

485   likely attributed to the presence of ilmenite. This corresponds to previous studies conducted by Norrbo et

486   al. (2016), Andrade et al. (2008), as well as Vigier et al. (2021a-c; 2023), who suggested that Fe^{2+} behaves

487   as a luminescence quencher. Blue luminescence was believed to be associated with the interaction between

488   O^{2-} and Ti^{4+} ions (Evans, 1994; Wong et al., 1995b), followed by a later hypothesis of a charge transfer

489   process involving Ti^{4+} ions and certain defect-related centers (Lacovara et al., 1985; Mikhailik et al., 2005).

490   However, it was widely accepted that the blue luminescence (characterized by a broad emission band at

491   blue to green region) observed in sapphire under SWUV illumination is associated with the presence of Ti

492   impurities, which are classified as element-related defects (Vigier et al., 2021a, b). Thus, it is likely that

493   the blue luminescence reported in this work is associated with Ti impurities, whereas orange to red

494   luminescence seems to be associated with complex defect-related emission centers.

495   The correlation between the orange to red PL emission band (approx. 650 nm, Fig. 9 blue

496   lines) and orange to red luminescence in unheated sapphire (Fig. 8), as well as the blue emission band

497   (approximately 525 nm, Fig. 9, red lines) and blue luminescence in heated sapphire (Fig. 8), seem to

498   correspond with each other only in samples from the low-density-silk group (Fig. 9b). The high-density-

499   silk group exhibits a reduction in the emission band throughout the whole visible spectrum after heating,

500   corresponding to an inertness under LWUV and SWUV excitation (Fig. 9a). The significant increase in the

501   red emission band (Fig. 9c) of the silk-free group corresponds to an intense purplish red luminescence

502   under LWUV excitation after heating. Notably it also displays a strong blue luminescence under SWUV

503   excitation after heating despite the lack of a blue emission band; this is possibly due to the 325 nm excitation

504   laser used in our PL investigation. Due to absorption-emission conditions, it is obvious that changing

505   excitation wavelengths have substantial impact on the observed emission. Even in the narrow range of 254,

506   325, or 365 nm UV excitation, significant differences in emission are expected. This was presented by

507   Wong et al. (1995a) and Vigier et al. (2023) whose sapphire emission band at 425 nm was obviously seen

508   only with a 254 nm excitation laser. By employing distinct SWUV (254 nm) and LWUV (365 nm)

509   excitation lasers, or even by conducting excitation spectroscopy, we may obtain more accurate results

510   compared to using a 325 nm laser only. Hence, the presence of orange to red luminescence and a broad

511   emission band at approximately 650 nm, along with blue luminescence and a broad emission band at around

512   525 nm, may serve as crucial indicators for distinguishing unheated and heated sapphire.

513

5 Conclusions

515   Overall, this work presents empirical evidence of the presence of melt inclusions (~ 1 µm in size) among

516   blue dots serving as new hint of heat treatment. Additionally, the study highlights the significance of

517   luminescence in distinguishing unheated sapphire from their heated counterparts.

518   Although the occurrence or disappearance of orange to red and blue luminescence has

519   not been conclusively elucidated, the F center (defect-related center) may be responsible for orange to red

520   luminescence, whereas the blue one may be attributed to Ti-impurities. Luminescence under SWUV and

521   LWUV excitation is likely seen only in sapphire with low Fe concentration (as supported by chemical

522   analysis), since we barely see luminescence in the group of high-density-silk sapphire samples. However,

523   the presence of orange to red luminescence under LWUV excitation may help in identifying unheated

524   sapphire. Blue luminescence under SWUV light can also serve as a useful indicator for identifying heated

525   sapphire since this luminescence, except for the high-density-silk group, is absent in all unheated sapphires

526   studied. This may be due to the interference-quenching effect of Fe^{2+}. In addition to blue, the presence of

527   purplish-red luminescence under LWUV light may also facilitate the identification of heated sapphire. For

528   the FTIR spectra, the 3309 cm^{-1} O-H stretching band alone seems to be insufficient to identify unheated or

529   heated sapphire since the effect of additional gas used during the heat treatment as well as the internal

530   diffusion may influence the appearance or absence of such an O-H feature. Also, an increase or elevated

531   intensity of the optical spectra at an absorption around 580 nm may indicate heated sapphire, as the majority

532   of heated sapphire samples exhibit a greater intensity in this band due to a higher number of Fe-Ti pairs,

533   derived from a decomposition of silk inclusions after heating.

534   Thus, combining blue luminescence (and/or purplish-red luminescence) with additional

535   analytical techniques represents a promising strategy for distinguishing unheated and heated sapphire.

536   Further studies should be conducted to explore the luminescence properties of sapphire originating from

537   different origins. This will contribute to a better understanding of the factors influencing the orange to red

538   and blue luminescence observed in these sapphire samples. It is also essential to turn attention on comparing

539   the luminescence characteristics shown by unheated and heated colored sapphire, as well as determining

540   the precise Fe and Ti concentration required to affect orange to red and blue luminescence. Furthermore,

541   to optimize the emission spectrum, it is recommended to utilize 254 nm laser excitation to obviously see a

542   shift of the emission band towards the blue region of heated sapphire.

543

544   *Author Contributions*. T.P., C.S., B.W., L.N. conducted conceptualization, E.G.Z. acquired samples, T.P.,

545   C.S., B.W., L.N., C.C.N., M.W., E.L., G.G., T.S. conducted analyses and evaluation, T.P. wrote the

546   manuscript, all co-authors reviewed and edited the manuscript.

547

548   *Competing interests*. The contact author has declared that none of the authors has any competing interests.

549

563 **6 References**

564 Alombert-Goget, G., Li, H., Guyot, Y., Brenier, A., and Lebbou, K.: Luminescence and coloration of
565   undoped and Ti-doped sapphire crystals grown by Czochralski technique, J. Lumin., 169, 516-519,
566   https://doi.org/10.1016/j.jlumin.2015.02.001, 2016a.
567 Alombert-Goget, G., Li, H., Faria, J., Labor, S., Guignier, D., and Lebbou, K.: Titanium distribution in
568   Ti-sapphire single crystals grown by Czochralski and Verneuil technique, Opt. Mater., 51, 1-4,
569   https://doi.org/10.1016/j.optmat.2015.11.016, 2016b.
570 Ananthakumar, S., Krishnapriya, G., Damodaran, A. D., and Warrier, K. G. K.: Thermal decomposition
571   characteristics of boehmite gels under microwave heating and associated microstructural features,
572   Mater. Lett., 35, 95-99, https://doi.org/10.1016/S0167-577X(97)00228-0, 1998.
573 Andrade, L. H. C., Lima, S. M., Novatski, A., Neto, A. M., Bento, A. C., Baesso, M. L., Gandra, F. C. G.,
574   Guyot, Y., and Boulon, G.: Spectroscopic assignments of Ti^{3+} and Ti^{4+} in titanium-doped OH-free
575   low silica calcium aluminosilicate glass and role of structural defects on the observed long lifetime
576   and high fluorescence of Ti^{3+} ions, Phys. Rev. B, 78, 224202,
577   https://doi.org/10.1103/PhysRevB.78.224202, 2008
578 Beran, A. and Rossman, G. R.: OH in naturally occurring corundum, Eur. J. Mineral., 18, 441-447,
579   https://doi.org/10.1127/0935-1221/2006/0018-0441, 2006.
580 Cartier, L. E.: Ruby and sapphire from marosely, Madagascar, J. Gemmol., 31, 171-180,
581   http://doi.org/10.15506/JoG.2009.31.5.171, 2009.
582 Choi, E., Song, K., An, S., Lee, K., Youn, M., Park, K., Jeong, S., and Kim, H.: Cu/ZnO/AlOOH catalyst
583   for methanol synthesis through CO_2 hydrogenation, Korean J. Chem. Eng., 35, 73-81,
584   https://doi.org/10.1007/s11814-017-0230-y, 2018.
585 Crowningshield, R.: Developments and highlights at the gem trade lab in new york: Unusual items
586   encountered (sapphire with unusual fluorescence), Gems Gemol., 12, 73, 1966.
587 Crowningshield, R.: Developments and highlights at GIA's lab in New York: Unusual fluorescence,
588   Gems Gemol., 13, 120-122, 1970.

25

589 Delattre, S., Balan, E., Lazzeri, M., Blanchard, M., Guillaumet, M., Beyssac, O., Haussühl, E., Winkler,
590   B., Salje, E. K. H., and Calas, G.: Experimental and theoretical study of the vibrational properties
591   of diaspore (α-AlOOH), Phys. Chem. Miner, 39, 93-102, https://doi.org/10.1007/s00269-011-
592   0464-x, 2012.

593 Dubinsky, E. V., Stone-Sundberg, J., and Emmett, J. L.: A quantitative description of the causes of color
594   in corundum, Gems Gemol., 56, 2-28, https://doi.org/10.5741/gems.56.1.2, 2020.

595 Ediriweera, R. and Perera, S.: Heat treatment of geuda stones - spectral investigation, J. Gemmol., 21,
596   403-410, https://doi.org/10.15506/jog.1989.21.7.403, 1989.

597 Emmett, J. L. and Douthit, T. R.: Heat treating the sapphires of Rock Creek, Montana, Gems Gemol., 29,
598   250-272, https://doi.org/10.5741/gems.29.4.250, 1993.

599 Emmett, J. L., Scarratt, K., McClure, S. F., Moses, T., Douthit, T. R., Hughes, R., Novak, S., Shigley, J.
600   E., Wang, W., Bordelon, O., and Kane, R. E.: Beryllium diffusion of ruby and sapphire, Gems
601   Gemol., 39, 84-135, https://doi.org/10.5741/gems.39.2.84, 2003.

602 Evans, B. D.: Ubiquitous blue luminescence from undoped synthetic sapphire, J. Lumin., 60-61, 620-626,
603   https://doi.org/10.1016/0022-2313(94)90233-X, 1994.

604 Ferguson, J. and Fielding, P. E.: The origins of the colors of yellow, green and blue sapphires, Chem.
605   Phys. Lett., 10, 262-265, https://doi.org/10.1016/0009-2614(71)80282-8, 1971.

606 Ferguson, J. and Fielding, P. E.: The origins of the colors of natural yellow, blue, and green sapphires,
607   Aust. J. Chem., 25, 1371-1385, https://doi.org/10.1071/CH9721371, 1972.

608 Filatova, N. V., Kosenko, N. F., and Artyushin, A. S.: The physicochemical analysis of bayerite $Al(OH)_3$
609      $\rightarrow \gamma\text{-}Al_2O_3$ transformation, J. Sib. Fed. Univ. Chem., 14, 527-538, https://doi.org/10.17516/1998-
610   2836-0260, 2021.

611 Fritsch, E., Chalain, J. P., Hanni, H., Devouard, B., Chazot, G., Giuliani, G., Schwartz, D., Rollion-Bard,
612   C., Garnier, V., Barda, S., Ohnenstetter, D., Notari, F., and Maitrallet, P.: Le nouveau traitement
613   produisant des couleurs orange a jaune dans les saphirs, Revue de Gemmologie n° 147-Février
614   2003, 147, 11-23, 2003.

615 Gog, H. V.: First-principles study of dehydration interfaces between diaspore and corundum, gibbsite and
616   boehmite, and boehmite and $\gamma\text{-}Al_2O_3$: Energetic stability, interface charge effects, and dehydration
617   defects, Appl. Surf. Sci., 541, 148501, https://doi.org/10.1016/j.apsusc.2020.148501, 2021.

618 Häger, T.: Farbgebende und "farbhemmende" Spurenelemente in blauen Saphiren, Berichte der
619   Deutschen Mineralogischen Gesellschaft - Beih. Eur. J. Mineral., 4, 109, 1992.

620 Häger, T.: High temperature treatment of natural corundum, in: Proceeding of the International Workshop
621   on Material Characterization by Solid State Spectroscopy: The Minerals of Vietnam, Hanoi, 4-10
622   April 2001, 1-10, 2001.

623 Hughes, E. B. and Perkins, R.: Madagascar sapphire: Low temperature heat treatment experiments, Gems
624   Gemol., 55, 184-197, http://doi.org/10.5741/GEMS.55.2.184, 2019.

625 Hughes, R. W. (1st edn.): Ruby & Sapphire, RWH Publishing, 511 pp., ISBN 0964509768, 1997.

626 Hughes, R. W.: Ruby & sapphire: A gemologist's guide, RWH Publishing/Lotus Publishing, 816 pp.,
627   ISBN 9780964509719, 2017.

628   Jaliya, R. G. C., Dharmaratne, P. G. R., and Wijesekara, K. B.: Characterization of heat treated geuda
629   gemstones for different furnace conditions using FTIR, XRD and UV-Visible spectroscopy
630   methods, Solid Earth Sci., 5, 282-289, https://doi.org/10.1016/j.sesci.2020.11.001, 2020.
631   Jung, I. H., Eriksson, G., Wu, P., and Pelton, A.: Thermodynamic modeling of the Al_2O_3–Ti_2O_3–TiO_2
632   system and its applications to the Fe–Al–Ti–O inclusion diagram, ISIJ INT., 49, 1290-1297,
633   https://doi.org/10.2355/isijinternational.49.1290, 2009.
634   Kammerling, R. C., Koivular, J. I., and Kane, R. E.: Gemstone enhancement and its detection in the
635   1980s, Gems Gemol., 26, 32-49, https://doi.org/10.5741/GEMS.26.1.32, 1990.
636   Kane, R. E.: The gemological properties of Chatham flux-grown synthetic orange sapphire and synthetic
637   blue sapphire, Gems Gemol., 18, 140-153, https://doi.org/10.5741/GEMS.18.3.140, 1982.
638   Kloprogge, J. T., Ruan, H. D. and Frost, R. L.: Thermal decomposition of bauxite minerals: infrared
639   emission spectroscopy of gibbsite, boehmite and diaspore, J. Mater. Sci., 37, 1121-1129,
640   https://doi.org/10.1023/A:1014303119055, 2002.
641   Krebs, J. J. and Maisch, W. G.: Exchange effects in the optical-absorption spectrum of Fe^{3+} in Al_2O_3,
642   Phys. Rev. B, 4, 757-769, https://doi.org/10.1103/PhysRevB.4.757, 1971.
643   Kyi, U. H., Buchhol, P., and Wolf, D.: Heat treatment of milky sapphires from the Mogok stone tract,
644   Myanmar, J. Gemmol., 26, 313-315, https://doi.org/10.15506/jog.1999.26.5.313, 1999.
645   Lacovara, P., Esterowitz, L., and Kokta, M.: Growth, spectroscopy, and lasing of titanium-doped
646   sapphire, IEEE J. Quantum Electron., 21, 1614-1618, https://doi.org/10.1109/JQE.1985.1072563,
647   1985.
648   Mattson, S. M. and Rossman, G. R.: Fe^{2+}-Ti^{4+} charge transfer in stoichiometric Fe^{2+},Ti^{4+}-minerals, Phys.
649   Chem. Miner., 16, 78-82, https://doi.org/10.1007/BF00201333, 1988.
650   McClure, D. S.: Optical spectra of transition-metal ions in corundum, J. Chem. Phys., 36, 2757-2779,
651   https://doi.org/10.1063/1.1732364, 1962.
652   McClure, S. F. and Smith, C. P.: Gemstone enhancement and detection in the 1990s, Gems Gemol., 36,
653   336-539, http://doi.org/10.5741/GEMS.36.4.336, 2000.
654   McClure, S. F., Kane, R. E., and Sturman, N.: Gemstone enhancement and detection in the 2000s, Gems
655   Gemol., 46, 218-240, http://doi.org/10.5741/GEMS.46.3.218, 2010.
656   Mikhailik, V. B., Kraus, H., Wahl, D., and Mykhaylyk, M. S.: Luminescence studies of Ti-doped Al_2O_3
657   using vacuum ultraviolet synchrotron radiation., Appl. Phys. Lett., 86, 101909,
658   http://doi.org/10.1063/1.1880451, 2005.
659   Monarumit, N., Lhuaamporn, T., Wathanakul, P., Saiyasombat, C., and Wongkokua, W.: The acceptor-
660   donor pair recombination of beryllium-treated sapphires, Radiat. Phys. Chem., 206, 110756,
661   https://doi.org/10.1016/j.radphyschem.2023.110756, 2023.
662   Moon, A. R. and Phillips, M. R.: Defect clustering and color in Fe,Ti: α-Al_2O_3, J. Am. Ceram. Soc., 77,
663   356-367, https://doi.org/10.1111/j.1151-2916.1994.tb07003.x, 1994.
664   Nassau, K.: The causes of color, Sci. Am., 243, 124-154,
665   https://doi.org/10.1038/SCIENTIFICAMERICAN1080-124, 1980.
666   Nassau, K.: Heat treating ruby and sapphire: Technical aspects, Gems Gemol., 17, 121-131,
667   https://doi.org/10.5741/GEMS.17.3.121, 1981.

668 Nelson, D. F. and Sturge, M. D.: Relation between absorption and emission in the region of the R lines of
669   ruby, Phys. Rev., 137, A1117-A1130, https://doi.org/10.1103/PhysRev.137.A1117, 1965.
670 Nikolskaya, L. V., Terekhova, V. M., and Samoilovich, M. I.: On the origin of natural sapphire color,
671   Phys. Chem. Miner., 3, 213-224, https://doi.org/10.1007/BF00633571, 1978.
672 Norrbo, I., Gluchowski, P., Hyppänen, I., Laihinen, T., Laukkanen, P., Mäkelä, J., Mamedov, F., Santos,
673   H. S., Sinkkonen, J., Tuomisto, M., Viinikanoja, A., and Lastusaari, M.: Mechanisms of
674   tenebrescence and persistent luminescence in synthetic hackmanite $Na_8Al_6Si_6O_{24}(Cl,S)_2$, ACS
675   Appl. Mater. Interfaces, 8, 11592-11602, https://doi.org/10.1021/acsami.6b01959, 2016.
676 Notari, F., Fritsch, E., and Grobon, C.: Comment l'observation de la luminescence (fuorescence) peut
677   aider a l'identification des corindons jaunes, rose orange et orange, traites par diffusion du
678   beryllium (How the observation of luminescence might aid in the identification of yellow, orangy
679   pink and orange corundum treated by Be-diffusion), Rev. de Gem., 148, 40-43, 2003.
680 Notari, F., Hainschwang, T., Caplan, C., and Ho, K.: The heat treatment of corundum at moderate
681   temperature, InColor, 42, 15-23, 2018.
682 Page, P. S., Dhabekar, B. S., Bhatt, B. C., Dhoble, A. R., and Godbole, S. V.: Role of Ti^{4+} in the
683   luminescence process of Al_2O_3:Si,Ti, J. Lumin., 130, 882-887,
684   https://doi.org/10.1016/j.jlumin.2009.12.029, 2010.
685 Palanza, V., Di Martino, D., Paleari, A., Spinolo, G., and Loredana, P.: Micro-Raman spectroscopy
686   applied to the study of inclusions within sapphire, J. Raman Spectrosc., 39, 1007-1011,
687   https://doi.org/10.1002/jrs.1939, 2008.
688 Palke, A. C., Saeseaw, S., Renfro, N. D., Sun, Z., and McClure, S. F.: Geographic origin determination of
689   blue sapphire, Gems Gemol., 55, 536-579, https://doi.org/10.5741/gems.55.4.536, 2019.
690 Peiris, B. P. S.: Color enhancement of diesal geuda, in: Proceedings of the National symposium on geuda
691   heat treatment, Sri Lanka, 10-11 June 1993, 113-122, 1993.
692 Perera, S. Z., Pannila, A. S., Gunasekera, H. P. N. J., and Ediriweera, R. N.: Anomalous behaviour of
693   certain geuda corundums during heat treatment, J. Gemmol., 22, 405-407,
694   https://doi.org/10.15506/jog.1991.22.7.405, 1991.
695 Perera, I.: Identification of treatable geuda by spectral investigations, in: Proceedings of the National
696   symposium on geuda heat treatment, Sri Lanka, 10-11 June 1993, 89-98, 1993
697 Pisutha-Arnond, V.: Ruby & sapphire treatments and identification: Decades of advancement, Amarin
698   Printing and Publishing, Bangkok, 96 pp., ISBN 978-6169145097, 2017.
699 Saeseaw, S., Kongsomart, B., Atikarnsakul, U., Khowpong, C., Vertriest, W., and Soonthorntantikul, W.:
700   Update on "low temperature" heat treatment of Mozambican ruby: A focus on inclusions and
701   FTIR spectroscopy. News from research, Gemological Institute of America, 37 pp., 2018.
702 Saeseaw, S., Khowpong, C., and Vertriest, W.: Low temperature heat treatment of pink sapphires from
703   Ilakaka, Madagascar, Gems Gemol., 56, 448-457, http://doi.org/10.5741/GEMS.56.4.448, 2020.
704 Samadhi, T., Subagjo, S., Lismana, K., and Fuadi, K.: Synthesis of γ-Al_2O_3 catalyst support from kaolin
705   of Indonesian origin. ITB J. Eng. Sci., 43, 113-126,
706   https://dx.doi.org/10.5614/itbj.eng.sci.2011.43.2.3, 2011.

707 Schmetzer, K. and Kiefert, L.: Spectroscopic evidence for heat treatment of blue sapphires from Sri
708   Lanka-additional data, J. Gemmol., 22, 80-82, 1990.

709 Segura, O.: La luminescence orange des corindons, Diplome Universitaire de Gemmologie de Nantes, 60
710   pp., 2013.

711 Sifontes, Á. B., Ávila, E., Gutiérrez, B., Rengifo, M., Mónaco, A., Díaz, Y., and Llovera, L.: Relevant
712   aspects of the biosynthesis of porous aluminas using glycosides and carbohydrates as biological
713   templates, Biotechnol. Res. Innov., 3, 22-37, https://doi.org/10.1016/j.biori.2019.01.004, 2019.

714 Smith, C. P.: A contribution to understanding the infrared spectra of rubies from Mong Hsu, Myanmar, J.
715   Gemmol., 24, 321-335, http://doi.org/10.15506/JoG.1995.24.5.321, 1995.

716 Soonthorntantikul, W., Khowpong, C., Atikarnsakul, U., Saeseaw, S., Sangsawong, S., Vertriest, W., and
717   Palke, A.: Observations on the heat treatment of basalt-related blue sapphires. News from
718   research, Gemological Institute of America, 60 pp., 2019.

719 Soonthorntantikul, W., Atikarnsakul, U., and Vertriest, W.: Blue sapphires from Mogok, Myanmar: A
720   gemological review, Gems Gemol., 57, 292-317, https://doi.org/10.5741/GEMS.57.4.292, 2021.

721 Soysa, E. S. K. and Fernando, W. S.: A field classification of low value corundum in Sri Lanka, J. Natn.
722   Sci. Coun. Sri Lanka, 20, 51-57, https://doi.org/10.4038/jnsfsr.v20i1.8058, 1992.

723 Spencer, L. J.: South African occurrences of willemite. Fluorescence of willemite and some other zinc
724   minerals in ultra-violet rays, Mineral. Mag., 21, 388-396,
725   https://doi.org/10.1180/minmag.1927.021.119.04, 1927.

726 Sripoonjan, T., Lhuaamporn, T., Nilhud, N., Sukkee, N., and Sutthirat, C.: Characteristics of Cyangugu
727   sapphire from rwanda, in: Proceedings of the 4th international gem and jewelry conference
728   (GIT2014) Chiang Mai, Thailand, 165-168, 2014.

729 Strange, L., Zhang, Y., Son, J., Gao, J., Joshi, V., and Yu, X. Y.: Aluminum hydroxide, bayerite,
730   boehmite, and gibbsite ToF-SIMS spectra in the negative ion mode. I. Surf. Sci. Spectra, 29,
731   025001. https://doi.org/10.1116/6.0001935, 2022.

732 Sun, T., Zhuo, Q., Chen, Y., and Wu, Z.: Synthesis of boehmite and its effect on flame retardancy of
733   epoxy resin, High Perform. Polym., 27, 1, 100-104, https://doi.org/10.1177/0954008314540312,
734   2015.

735 Sutthirat, C., Pattamalai, K., Sakkaravej, S., Pumpeng, S., Pisutha-Arnond, V., Wathanakul, P., Atichat,
736   W., and Sriprasert, B.: Indications of heating in corundum from experimental results, Gems
737   Gemol., 42, 86, 2006.

738 Themelis, T. (3rd edn.): The heat treatment of ruby & sapphire: Experiments & observations, Ted
739   Themelis, 294 pp., ISBN 0940965577, 2018.

740 Townsend, M. G.: Visible charge transfer band in blue sapphire, Solid State Commun., 6, 81-83,
741   https://doi.org/10.1016/0038-1098(68)90005-7, 1968.

742 Vigier, M. and Fritsch, E.: More on orange luminescence in corundum, Gems Gemol., 58, 376-377, 2022.

743 Vigier, M., Fritsch, E., and Segura, O.: Orange luminescence of corundum as a source of geologic
744   information?, Goldschmidt 2021 Abstract, Virtual conference, 4-9 July 2021,
745   https://doi.org/10.7185/gold2021.3467, 2021a.

29

746   Vigier, M., Fritsch, E., and Segura, O.: Orange luminescence of corundum an atypical origin for
747   gemmologists (part one), Revue de L'Association Française de Gemmologie N° 211-Mars 2021,
748   12-19, 2021b.
749   Vigier, M., Fritsch, E., and Segura, O.: Orange luminescence of corundum an atypical origin for
750   gemmologists (part two), Revue de L'Association Française de Gemmologie N° 212-Juin 2021,
751   13-19, 2021c.
752   Vigier, M., Fritsch, E., Cavignac, T., Latouche, C., and Jobic, S.: Shortwave UV blue luminescence of
753   some minerals and gems due to titanate groups, Minerals, 13, 104,
754   https://doi.org/10.3390/min13010104, 2023.
755   Vlaskin, M. S., Grigorenko, A. V., Zhuk, A. Z., Lisitsyn, A. V., Sheindlin, A. E., and Shkol'nikov, E. I.:
756   Synthesis of high-purity α-Al_2O_3 from boehmite obtained by hydrothermal oxidation of aluminum,
757   High Temp., 54, 322-329, https://doi.org/10.1134/S0018151X16020231, 2016.
758   Webster, R. (6th edn.): Practical gemmology. A study of the identification of gemstones, pearls, and
759   ornamental minerals, N.A.G. Press, Suffolk, USA, 92 pp., 1984.
760   Wong, W. C., McClure, D. S., Basun, S. A., and Kokta, M. R.: Charge-exchange processes in titanium-
761   doped sapphire crystals. I. Charge-exchange energies and titanium-bound excitons, Phys. Rev. B
762   Condens. Matter, 51, 5682-5692, https://doi.org/10.1103/physrevb.51.5682, 1995a.
763   Wong, W. C., McClure, D. S., Basun, S. A., and Kokta, M. R.: Charge-exchange processes in titanium-
764   doped sapphire crystals. II. Charge-transfer transition states, carrier trapping, and detrapping,
765   Phys. Rev. B Condens. Matter, 51, 5693-5698, https://doi.org/10.1103/physrevb.51.5693, 1995b.
766   Zeug, M., Nasdala, L., Wanthanachaisaeng, B., Balmer, W.A., Corfu, F., and Wildner, M.: Blue zircon
767   from Ratanakiri, Cambodia, J. Gemmol., 36, 112-132,
768   http://dx.doi.org/10.15506/JoG.2018.36.2.112, 2018.
769   Zeug, M., Nasdala, L., Chanmuang N., C., and Hauzenberger, C.: Gem topaz from the Schneckenstein
770   crag, Saxony, Germany: Mineralogical characterization and luminescence, Gems Gemol., 58, 2-
771   17, https://doi.org/10.5741/GEMS.58.1.2, 2022.